ELEVENTH EUROPEAN ROTORCRAFT FORUM

Paper No. 62

NOTES REGARDING FUNDAMENTAL UNDERSTANDINGS OF ROTORCRAFT AEROELASTIC INSTABILITY

Richard L. Bielawa

Rensselaer Polytechnic Institute
Troy, New York 12180-3590

September 10-13, 1985
London, England

THE CITY UNIVERSITY, LONDON, ECIV OHB, ENGLAND

NOTES REGARDING FUNDAMENTAL UNDERSTANDINGS OF ROTORCRAFT AEROELASTIC INSTABILITY

by

Richard L. Bielawa
Associate Professor
Department of Mechanical Engineering,
Aeronautical Engineering & Mechanics
Rensselaer Polytechnic Institute
Troy, New York 12180-3590

Abstract

An expanded description of the Force-Phasing Matrix (FPM) technique for understanding the physics of instabilities of linear dynamic systems is presented. The technique is a mathematically formalized procedure for identifying those forces acting on the system's component degrees-of-freedom which are in-phase with the velocities of these degrees-of-freedom. The FPM technique, originally defined only for the case of linear systems with constant coefficient, is expanded to the case with periodic coefficients. The technique is thus particularly well-suited to rotorcraft instability problems. Application of the technique is made to the cases of air resonance and blade flap-lag instabilities. Significant differences between ground resonance and air resonance instabilities, as identified using the FPM technique, are discussed. Finally, results obtained from applying the technique to the problem of flap-lag instability of a rotor in forward flight are also discussed.

1. Introduction

1.1 Background

In recent years considerable effort has been spent in the development of analyses for predicting aeroelastic and aeromechanical instabilities of helicopter rotor blades. To a great extent this cumulative effort has been well-directed; several aeroelastic stability analyses [1-3] have been formulated which successfully identify and model various types of rotor instability. Such analyses generally involve the derivation and solution of sets of linear differential equations describing the motion of the several degrees-of-freedom defining the total dynamic system. These multi-degree-of-freedom equations of motion are generally written in matrix form as:

$$[M]\{\ddot{x}\} + [C]\{\dot{x}\} + [K]\{x\} = \{F(t)\} \qquad (1)$$

A recognized hallmark of rotary-wing dynamics is an abundance of nonconservative forces (usually involving rotor speed). Consequently, the resulting analyses produce equations of motion of the above type wherein the M, C and K matrices (mass, damping and stiffness matrices, respectively) are square, real-valued, highly nonsymmetrical and often periodic in time. The universal starting point for rotary-wing stability analysis is to solve Eq.(1) as some form of an eigenvalue problem with the applied loading description (the right-hand side) set to zero.

The principal mathematical result of such an eigenvalue analysis is the eigenvalue itself which gives a quantitative measure of the stability level of the dynamic system as a whole. Hence, a ubiquitous characteristic inherent in all such aeroelastic analyses is a wealth of stability boundaries, as gleaned from the interpretations of the eigenvalues obtained, showing trends with respect to a multiplicity of system parameters. All too lacking, however, is a unifying exposition of the destabilizing mechanisms involved. Knowledge of such mechanisms has the potential for providing general insight into the physics and, thereby, enabling an efficient remedy to the instability to be devised. In addition to the system of equations and the resulting eigenvalues, recourse must be made to the eigenvectors to achieve this objective. It should be noted that as a rule, eigenvector information is typically discarded as a useless by-product or, at best, underutilized in most rotary-wing aeroelastic stability analyses. The primary tool advanced herein for providing insight into the destabilizing mechanisms is the "Force-Phasing Matrix" (FPM) methodology, as originally proposed in Ref.4 and later in Ref.5

1.2 Objectives

The primary objectives of this paper are twofold: First, since the original exposition of the force-phasing matrix technique little use has been made of the method. This has been due in part to the fact that it is not widely known and in part because it was originally formulated for the limited class of eigenvalue problems wherein the M, C and K matrices are constant. Thus, the first objective of this paper is to reacquaint the rotary-wing dynamics community to the method with appropriate reformulations, including the extension to Floquet type problems. The second objective of this paper is to provide new insights into contemporary rotary-wing instability issues as obtained using the reformulated Force-Phasing Matrix technique. As originally described in Refs.4 and 5 the FPM technique successfully identified the destabilizing elements in the matrix equations of motion only for the important but already well-understood problems of blade bending-torsion flutter and divergence. Results presented herein include applications of the FPM technique to helicopter air resonance and blade flap-lag instability.

2. Theoretical Development

2.1 Basic Ideas

The theoretical development of the FPM technique follows from three simple ideas governing the unstable motion of any linear multi-degree-of-freedom system: (1) The nature of any unstable system is that it has destabilizing forces acting on it which have components in-phase with velocity. Thus, for unstable motion these forces produce work on the system. (2) Within any such unstable dynamic system each degree-of-freedom has a multiplicity of forces which have components correspondingly in-phase with the velocity of that degree-of-freedom. Such forces are herein denoted as "driving forces." That each degree-of-freedom has drivers in a condition of instability is presented without proof, but follows heuristically from the properties of linear differential equations. (3) For any instability involving two or more degrees-of-freedom there will exist a multiplicity of energy-flow paths (i.e., vicious circles) wherein the two or more degrees-of-freedom will mutually "pump" energy into each other.

The principal function of the FPM technique is to identify those force terms in the equations of motion which, for an unstable mode, are so phased by the mode shape (eigenvector) as to be "drivers" of the motion. The technique is perhaps nothing more than a formalization of the intuitive use an experienced dynamicist would make of the eigenvector information. The basis of the technique can be seen by considering the eigensolution of Eq.(1) wherein the M, C and K matrices are assumed to be constant and the right-hand side is equated to zero. For this case the general solution to the homogeneous differential equation is:

$$\{x\} = \sum_{k} \{\varphi^{(k)}\}\, e^{\lambda_k t} \tag{2}$$

where λ_k denotes the kth eigenvalue and $\{\varphi^{(k)}\}$ denotes the corresponding kth eigenvector. In general, both λ_k and $\varphi^{(k)}$ are complex-valued. The eigenvalues $\lambda(= \sigma \pm i\omega)$, which give stability level (σ) and natural frequency (ω) information, are obtained from any of a current variety of standard eigensolution techniques. Upon inserting the general solution, Eq.(2), into the eigenvalue equations, each row of the resulting equation set represents the equilibrium of forces acting on a corresponding degree-of-freedom. Each such equation can be written as the sum of the mass, damper and spring forces of the nth diagonal element degree-of-freedom along with the remainder of the terms lumped together as a combined excitation force, f_n:

$$m_{nn}\lambda_k^2\varphi_n^{(k)} + c_{nn}\lambda_k\varphi_n^{(k)} + k_{nn}\varphi_n^{(k)} + \underbrace{\sum_{j\neq n} (m_{nj}\lambda_k^2 + c_{nj}\lambda_k + k_{nj})\varphi_j^{(k)}}_{f_n} = 0 \tag{3}$$

For the usual, nonpathological case m_{nn}, c_{nn} and k_{nn} are all positive numbers; that is, each autogenous mass (i.e., when uncoupled from the others) is generally a stable spring-mass-damper system. Since the eigenvalue λ_k is generally complex, Eq.(3) can then be interpreted as the sum of four complex quantities or vectors in the complex plane which must, furthermore, be in equilibrium. Assuming that for any complex pair the eigenvector with the positive imaginary part is used throughout, the argument of the eigenvector θ_k is the angle by which the inertia force vector is rotated (counterclockwise) relative to the damper force and the damper force is rotated relative to the stiffness force. For unstable motion the real part of λ_k (σ_k) is a positive number and, hence, θ_k will be less than $\frac{\pi}{2}$ (i.e., 90 degrees). If a point in time is taken when the velocity of the nth degree-of-freedom is pure real and positive, then the autogenous damper force $(-\lambda_k c_{nn}\varphi_n^{(k)})$ will correspondingly also be pure real but negative. Further, if it is recalled that the four vectors are in equilibrium and governed by the constraint on θ_k, then the real parts of the autogenous spring, damper and inertia forces will all be negative and, hence, the remaining lumped off-diagonal terms must always have a positive real part.

Figure 1, which demonstrates this argument, shows the four force vectors in the complex plane for an unstable oscillatory mode [$Re(\lambda_k) = \sigma_k > 0$; $\theta_k < \pi/2$] and unit negative real damping. Since the f_n vector is a sum of all the off-diagonal terms for the nth degree-of-freedom, any of the individual terms within f_n which has a positive real part must be deemed a "driver" for that degree-of-freedom. Conversely, any of the individual terms within f_n which has a negative real part can be deemed a "quencher" for that degree-of-freedom. This fact thus provides the dynamicist with the complementary information as to which parameters might be increased to stabilize an instability.

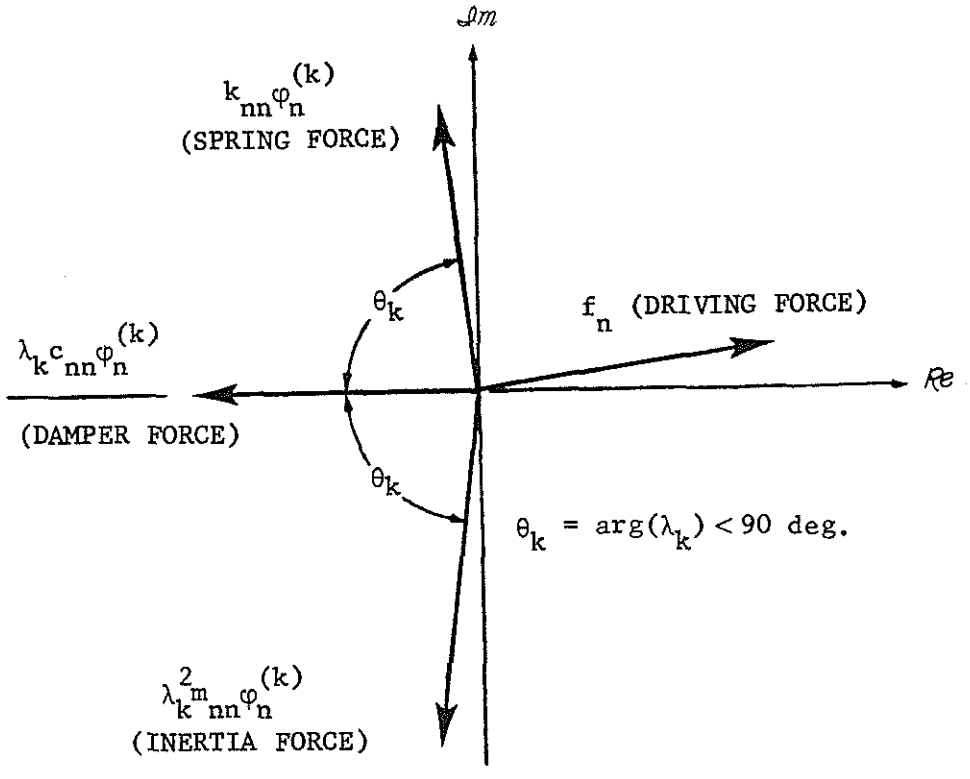

Figure 1 Force Vector Diagram for nth Degree-of-Freedom, kth Mode

The above interpretations of unstable motion can be quantitatively implemented by forming herein defined "force-phasing matrices." For any unstable eigenvalue λ_k these matrices have a one-to-one correspondence to the original M, C and K system matrices defining the equations of motion [Eq.(1)]: Any positive real element in one of the force-phasing matrices signifies that the corresponding system matrix element is a driver.

2.2 Mathematical Implementation-Constant Coefficient Case

Force-phasing matrices are essentially formed by dividing each row of the original system of equations by a number which renders the diagonal damping term pure negative real. For the case of constant coefficient matrices this can be easily accomplished using the eigenvalue and eigenvector information. The force-phasing matrices corresponding to the M, C and K system matrices, for the kth eigenvalue can be written, respectively as:

$$[P_M^{(k)}] = [p_{M_{ij}}^{(k)}] = -\,\mathrm{Re}\left[[m_{ij}] \textcircled{H} \left[\frac{\alpha_i^{(k)}}{\beta_i^{(k)} c_{ii}} \right] \right] \tag{4}$$

$$[P_C^{(k)}] = [p_{C_{ij}}^{(k)}] = -\,\mathrm{Re}\left[[c_{ij}] \textcircled{H} \left[\frac{\beta_j^{(k)}}{\beta_i^{(k)} c_{ii}} \right] \right] \tag{5}$$

$$[P_K^{(k)}] = [p_{K_{ij}}^{(k)}] = -\,\mathrm{Re}\left[[k_{ij}] \textcircled{H} \left[\frac{\gamma_j^{(k)}}{\beta_i^{(k)} c_{ii}} \right] \right] \tag{6}$$

where the Ⓗ symbol denotes a Hadamard matrix multiplication (Ref.6).

The $\alpha^{(k)}$, $\beta^{(k)}$ and $\gamma^{(k)}$ vectors are formed from the results of the basic eigensolution:

$$\{\alpha^{(k)}\} = \lambda_k^2 \{\varphi^{(k)}\} \tag{7}$$

$$\{\beta^{(k)}\} = \lambda_k \{\varphi^{(k)}\} \tag{8}$$

$$\{\gamma^{(k)}\} = \{\varphi^{(k)}\} \tag{9}$$

Note that this formulation is general in that it covers both oscillatory and aperiodic instabilities. Although not strictly required for the methodology, the division by c_{ii} in Eqs.(4), (5) and (6) serves the useful normalization of the matrices relative to the diagonal damping terms. Clearly, this division will render all diagonal terms in $[P_C^{(k)}]$ equal to -1.

2.3 Mathematical Implementation - Periodic Coefficient Case

The extension of the FPM technique to the case wherein the system matrices [M, C and K of Eq.(1)] are periodic in time (Floquet theory) requires again a basic eigenvalue solution. In this case, however, the appropriate eigenvalue quantity is denoted the characteristic multiplier Λ_k which can be efficiently obtained using a transition matrix approach (see Ref.7). For present purposes the Floquet theory problem is given in non-dimensional form as:

$$\{\overset{*}{y}\} = [A(\psi)]\{y\} \tag{10}$$

where $(\overset{*}{})$ denotes differentiation with respect to nondimensional time ψ ($= \Omega t$, where $\Omega = 2\pi/T$), and $[A(\psi)]$ and $\{y\}$ result from an augmented state vector representation of the basic dynamic equation:

$$\left\lfloor \overset{*}{y} \right\rfloor = \left\lfloor \overset{*}{x} \;\vdots\; x \right\rfloor \tag{11}$$

$$[A(\psi)] = \left[\begin{array}{c:c} -[M]^{-1}[C(\psi)] & -[M]^{-1}[K(\psi)] \\ \hdashline I & 0 \end{array}\right] \tag{12}$$

The Floquet theory transition matrix approach generally involves the formation and eigensolution of a transition matrix $[\Phi_A(T,0)]$, as typically obtained using some form of numerical integration scheme (with step size h) over one period, T:

$$\{y(T)\} = [H(T-h)][H(T-2h)] \ldots [H(0)]\{y(0)\} \tag{13a}$$

$$= [\Phi_A(T,0)]\{y(0)\} = \Lambda\{y(0)\} \tag{13b}$$

where $\{y(0)\}$ is both the arbitrary state vector at the start of the period and the resulting eigenvector of the transition matrix. As shown in Appendix A, the H matrices of Eq.(13a) together with the eigenvector $\{y(0)\}$ enable the characteristic (nondimensional) acceleration, velocity and displacement vectors at $\psi = \psi_m$ to be represented as follows:

$$\{\overset{**}{x}(\psi_m)\} = [U_m^{(A)}]\{y(0)\} \tag{14a}$$

$$\{\overset{*}{x}(\psi_m)\} = [U_m^{(B)}]\{y(0)\} \tag{14b}$$

$$\{x(\psi_m)\} = [U_m^{(C)}]\{y(0)\} \tag{14c}$$

Using these $U_m^{(A)}$, $U_m^{(B)}$ and $U_m^{(C)}$ matrices the force-phasing matrices for the kth eigenvalue can then be written as:

$$[P_M^{(k)}] = -\frac{1}{N_p} \sum_{m=1}^{N_p}{}' \, Re\left[[m_{ij}(\psi_m)] \circledH \left[\frac{\alpha_{jm}^{(k)}}{\beta_{im}^{(k)} c_{ii}^{o}} \right] \right] \tag{15}$$

$$[P_C^{(k)}] = -\frac{1}{N_p} \sum_{m=1}^{N_p}{}' \, Re\left[[c_{ij}(\psi_m)] \circledH \left[\frac{\beta_{jm}^{(k)}}{\beta_{im}^{(k)} c_{ii}^{o}} \right] \right] \tag{16}$$

$$[P_K^{(k)}] = -\frac{1}{N_p} \sum_{m=1}^{N_p}{}' \, Re\left[[k_{ij}(\psi_m)] \circledH \left[\frac{\gamma_{jm}^{(k)}}{\beta_{im}^{(k)} c_{ii}^{o}} \right] \right] \tag{17}$$

where N_p is the number of intervals into which the period, T, is divided, as per Eq.(13a), c^o_{ii} is the constant part of the ith diagonal damping matrix element and where:

$$\{\alpha_m^{(k)}\} = [U_m^{(A)}]\{y^{(k)}(0)\} \tag{18}$$

$$\{\beta_m^{(k)}\} = [U_m^{(B)}]\{y^{(k)}(0)\} \tag{19}$$

$$\{\gamma_m^{(k)}\} = [U_m^{(C)}]\{y^{(k)}(0)\} \tag{20}$$

2.4 Use of Force-Phasing Matrices - Energy-Flow Paths

Using the above formulations force-phasing matrices can be written for either the constant coefficient case [Eqs.(4) - (6)] or the periodic coefficient case [Eqs.(15) - (17)]. In either case the force-phasing matrices constitute one-to-one correspondences with their respective dynamic system M, C and K matrices. The interpretation and usage of the force-phasing matrices can be summarized as follows:

(1) Identify the most active degrees-of-freedom from the eigenvector information for the unstable mode in question.

(2) Look for relatively large positive (+) values in the force-phasing matrices involving the most active degrees-of-freedom as identified from the eigenvector. Such elements are the "drivers" for the unstable motion.

(3) Of the drivers so identified look for those which involve degrees-of-freedom which mutually drive each other. Such drivers we denote as "critical drivers." As illustrated in Figure 2 such critical drivers would occur in the most simple form as off-diagonal terms involving two distinct degrees-of-freedom, say the nth and mth.

(4) Thus, critical drivers would show up as relatively large (+) values in both the $(\ )_{mn}$ and $(\ )_{nm}$ elements of one or more of the three force-phasing matrices. The interaction through these terms is defined herein as the "energy-flow path."

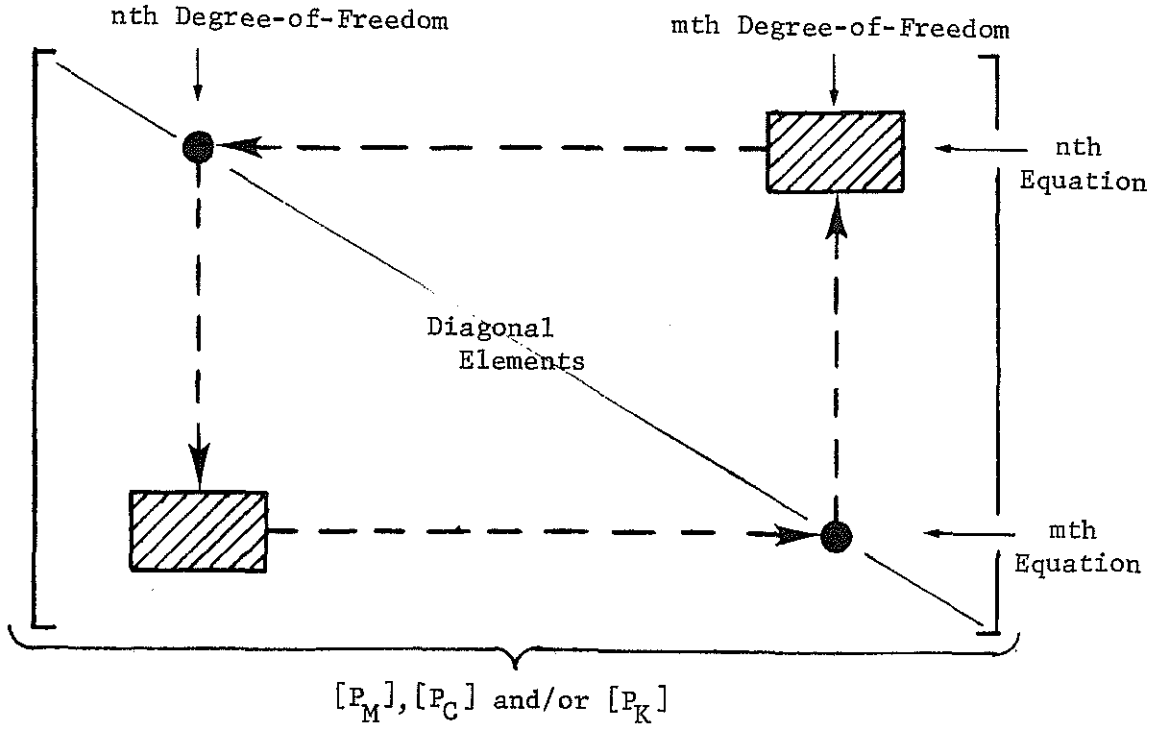

: Critical Drivers ≡ Terms in original dynamic equations acting as mutual drivers for unstable motion, as identified by (+) terms in corresponding force-phasing matrices.

: Energy-Flow Path

Figure 2 Definitions of Critical Drivers and Energy-Flow Path

3. Applications

The FPM technique is completely general in that it can be applied to any explicit set of linear (or linearized) differential equations of motion, irregardless of the number of degrees-of-freedom. For demonstration purposes herein, however, two basic sets of simplified equations are used for the instability phenomena to be examined. For ground and air resonance purposes the equations described in Ref.8 were selected because they constitute a reasonably representative modeling of the phenomena yet are sufficiently explicit for the purpose of demonstrating usage of the FPM technique. This set of equations, applicable to both ground and air resonance calculations, is reproduced in Appendix B. For the analysis of flap-lag instability in forward flight the differential equations defined by Peters (Ref.3) were selected; only selected portions of these equations are reproduced herein for brevity.

3.1 Ground Resonance

As can readily be seen from any typical set of basic ground resonance equations [8,9], the coupling terms producing the instability (i.e., those which couple the pylon (hub) in-plane translational displacement and rotor blade cyclic edgewise motion dynamic subsystems) can be readily identified to be the off-diagonal, acceleration dependent ones. Using the complex displacement scheme of Ref.9 and the nomenclature of the equations given in Appendix B, these coupling terms can be expressed as:

Hub in-plane motion ($z = x + iy$) equation

$$\ldots + \frac{b}{2} S_{48} \ddot{\varepsilon} + \ldots = 0 \tag{21a}$$

Rotor edgewise motion ($\varepsilon = e_x + i e_y$) equation

$$S_{48} \ddot{z} + \ldots = 0 \tag{21b}$$

where S_{48}, as defined in Appendix B, is a generalized edgewise first mass moment of inertia for the blade, and b is the number of blades. This parameter (S_{48}) is directly analogous to the μ parameter defined in the classic work of Coleman and Feingold (Ref.9). In the basic ground resonance equations of motion these coupling terms are quite literally the only ones present, and indeed (in the limit) minimization of these terms relative to the diagonal terms, eliminates the instability. Clearly, identifying the coupling terms in the above manner, however, is an insufficient explanation of the ground resonance instability. That these coupling terms result in instability is due in large measure to the phase relationships resulting between $\ddot{z}$ and $\ddot{\varepsilon}$, and even more importantly, between e_x and e_y. These issues are addressed in more detail in the following section.

3.2 Air Resonance

Appendix B presents the simplified set of equations used for examining the physics of the air resonance phenomenon. The minimum description selected for this simplified analysis includes eight (cyclic) degrees-of-freedom: longitudinal and lateral hub translations (x and y), hub roll and pitch rotations (θ_{x_f} and θ_{y_f}), blade longitudinal and lateral inplane bending (e_x and e_y), and blade rolling and pitching flatwise bending (θ_{x_R} and θ_{y_R}). The increased complexity of the air resonance equations (over those for ground resonance) is commensurate with the need to include aerodynamic as well as gravitational effects. Consequently, coupling terms abound in the air resonance equations.

For illustrative purposes the four-bladed, Froude-scaled hingeless rotor/airframe configuration described in Ref.8 was used. Table 1 lists the mechanical and geometrical properties of both the selected blade configuration and the (rigid body) airframe.

TABLE 1

AEROMECHANICAL PROPERTIES OF ROTOR AND PYLON
USED FOR AIR RESONANCE CASE

1. Rotor Properties	
(Nominal) tip speed, ΩR	90.50 m/s
Froude number @ nom ΩR	608.41
Radius, R	1.37 m
Mass distribution, m'	4.98 kg/m
Flatwise bending stiffness, EI_w	1.904 Nm^2
Edgewise bending stiffness, EI_v	106.65 Nm^2
(Nominal modal damping, ζ_v, ζ_w	0.005
Number of blades, b	4
Lock number, γ	5.854
C_T/σ (hover)	0.075
Chord, c	11.65 cm
Precone angle, β_B	0.5 deg
Collective angle, $\theta_{.75R}$	9.98 deg
Inflow, λ	-0.06371
a	0.1/deg
c_{d_o}	0.008
Thrust, T	387.20 N
2. Pylon Properties	
Pylon mass, m_f	37.02 kg
c.g. location, h_1	0.305 m
(Nominal) roll inertia, I_{φ_f}	0.163 kg-m^2
(Nominal) pitch inertia, I_{θ_f}	0.746 kg-m^2

For a hovering flight condition (ΩR = 96.01 m/s) an unstable air resonance eigenvalue pair (characteristic roots) was calculated to be $\lambda = +.2498 \pm i26.8127$. For this eigenvalue the complex eigenvector is given by:

		$\underline{x}$	$\underline{y}$	$\underline{\theta_{x_f}}$
$\lfloor\varphi\rfloor$ =	/Real/	-.2324	-.5604	.8284
	/Imag/	-.0476	-.0438	.1378

$\underline{\theta_{y_f}}$	$\underline{\epsilon_x}$	$\underline{\epsilon_y}$	$\underline{\theta_{x_R}}$	$\underline{\theta_{y_R}}$
-.2619	1.0000	.0219	-.4546	.0862
-.0651	0.	-.9853	-.4509	.1569

Based on this modal information the unstable motion is seen to involve principally the y, θ_{x_f}, ϵ_x, ϵ_y and θ_{x_R} degrees-of-freedom. These degrees-of-freedom constitute those defining lateral motion with almost equal components of both lateral and longitudinal cyclic blade edgewise bending. For the unstable air resonance characteristic root pair given above, the force-phasing matrices which were calculated using Eqs.(4), (5) and (6), are given below with the most significant drivers for the principal degrees-of-freedom indicated with boxes.

$[P_M]$, Phasing Matrix for Mass Matrix

-.907E+01	.000E+00	.000E+00	-.250E+02	.512E+02	.000E+00	.000E+00	-.330E+00
.000E+00	-.907E+01	-.790E+02	.000E+00	.000E+00	.101E+03	-.421E+00	.000E+00
.000E+00	.109E+00	-.173E-01	.000E+00	.000E+00	.449E-02	-.210E+00	.000E+00
.754E-01	.000E+00	.000E+00	-.209E-01	.358E-02	.000E+00	.000E+00	-.233E+00
-.312E+00	.000E+00	.000E+00	-.116E-01	-.187E+00	.000E+00	.000E+00	.000E+00
.000E+00	-.392E+01	-.157E+00	.000E+00	.000E+00	-.187E+00	.000E+00	.000E+00
.000E+00	.851E-03	.385E+00	.000E+00	.000E+00	.000E+00	-.472E-02	.000E+00
.151E-02	.000E+00	.000E+00	.559E+00	.000E+00	.000E+00	.000E+00	-.472E-02

$[P_C]$, Phasing Matrix for Damping Matrix

-.100E+01	-.115E+00	.718E+01	-.119E+01	.798E+01	-.178E+00	-.310E+01	.492E+00
.205E-01	-.100E+01	-.155E+01	-.961E+00	-.425E+00	-.189E+00	.875E+00	.240E+00
.211E-01	-.172E-02	-.100E+01	.798E+00	-.286E+00	.000E+00	.605E+00	-.332E+00
-.227E-02	-.154E+00	-.773E+01	-.100E+01	.000E+00	-.195E+00	.513E+01	.438E+00
.533E-01	-.213E-03	.359E+00	.000E+00	-.100E+01	-.229E+01	.239E+00	.000E+00
-.164E-04	-.730E-02	.000E+00	.260E-01	.236E+01	-.100E+01	.000E+00	.826E-01
-.235E-01	.173E-02	.108E+01	-.946E+00	.250E+00	.000E+00	-.100E+01	.710E+00
.222E-02	.130E+00	.759E+01	.103E+01	.000E+00	.107E+01	-.907E+01	-.100E+01

$[P_K]$, Phasing Matrix for Stiffness Matrix

.000E+00	.000E+00	.000E+00	.252E+01	.505E+00	-.206E+02	.394E+01	-.132E+02
.000E+00	.000E+00	.625E+01	.000E+00	.616E+00	.110E+01	-.170E+02	-.705E+00
.000E+00	.000E+00	-.706E-03	.000E+00	.000E+00	.738E+00	.000E+00	-.429E+00
.000E+00	.000E+00	.000E+00	-.706E-03	.546E+00	.000E+00	.314E+01	.000E+00
.000E+00	.000E+00	.000E+00	.000E+00	.793E+00	.257E+01	.000E+00	-.216E+00
.000E+00	.000E+00	.000E+00	.000E+00	.265E+01	.793E+00	-.640E+00	.000E+00
.000E+00	.000E+00	.000E+00	.000E+00	.000E+00	-.663E+00	-.261E-02	.213E+00
.000E+00	.000E+00	.000E+00	.000E+00	-.287E+01	.000E+00	.256E+01	-.261E-02

Using these force-phasing matrices together with the relative modal activity for this mode (as indicated above by the eigenvector information) an energy-flow diagram can be drawn. Such a diagram represents a summary of the information provided by the force-phasing matrices. The energy-flow diagram for the given air resonance condition is shown below.

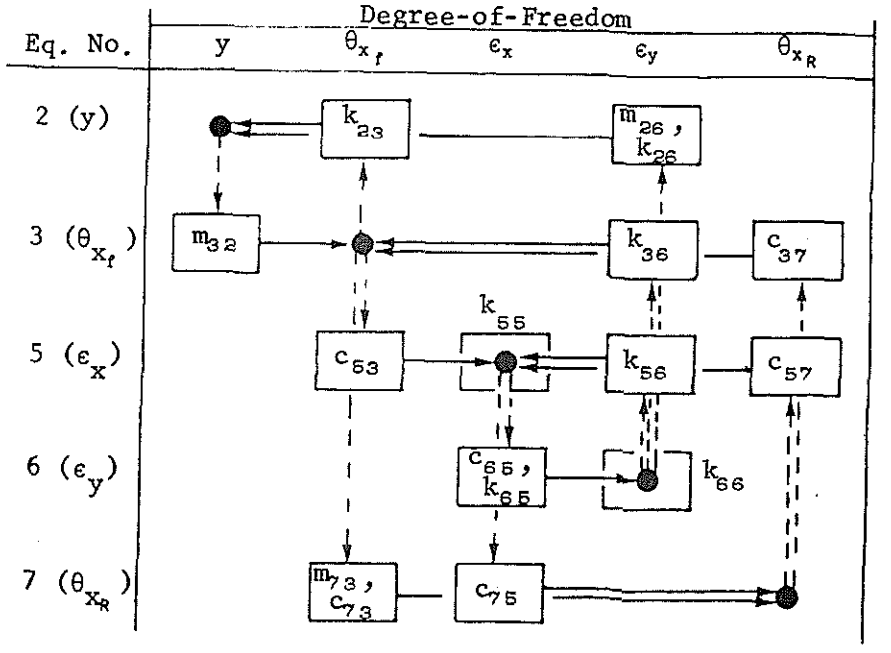

Figure 3 Energy-Flow Diagram for Air Resonance Instability Condition, Hovering Flight, $C_T/\sigma = 0.075$

The following observations and interpretations can be drawn from this diagram (together with the quantitative information contained in the actual force-phasing matrices):

- The air resonance instability is a multiple energy-flow path phenomenon with both direct and indirect paths.
- Contrary to the ground resonance case there are no pylon-to-blade edgewise acceleration dependent coupling terms participating in any of the energy-flow paths.
- Direct energy-flow paths exist between the following sets of degrees-of-freedom (y and θ_{x_f}), (θ_{x_f} and θ_{x_R}), (ϵ_x and ϵ_y), and (ϵ_x and (θ_{x_R}).
- Indirect energy-flow paths exist between θ_{x_f} and ϵ_y (through ϵ_x), and between y and ϵ_y (through θ_{x_f} and ϵ_x).
- The unstable coupling between ϵ_x and ϵ_y, which is typical with both ground resonance and air resonance, involves not only damping and stiffness off-diagonal terms, but the diagonal stiffness terms as well. The diagonal stiffness contributions are relatively small, however, and arise from the fact that the k_{55} and k_{66} terms themselves become negative for the supercritical operation characteristic of ground and air resonance phenomenon.
- The most significant critical drivers are those coupling forces associated with the k_{23}, m_{26}, k_{26}, m_{32}, k_{36}, c_{37}, c_{53}, k_{55}, k_{56}, c_{57}, c_{65}, k_{65}, k_{66}, m_{73}, c_{73} and c_{75} terms.

Using the equations in Appendix B, the critical drivers can be explicitly written and are given in the following table:

TABLE 2

CRITICAL DRIVERS FOR AIR RESONANCE HOVERING CONDITION

- Hub Lateral Force (F_y):

  k_{23}: $T\theta_{x_f}$

  m_{26}: $\frac{b}{2} S_{48}\ddot{\epsilon}_y$

  k_{26}: $-\frac{b}{2} K_a\Omega^2\beta_B(\lambda T_{19} + 2\theta_{.75R}T_{20})\epsilon_y$

- Hub Roll Moment (M_{x_f}):

  m_{32}: $-(b\beta_B S_1 - m_f h_1)\ddot{y}$

  k_{36}: $\frac{b}{2} K_a\Omega^2 R(\lambda T_{20} + 2\theta_{.75R}T_{21})\epsilon_y$

  c_{37}: $\frac{b}{2} K_a\Omega R T_{11}\dot{\theta}_{x_R}$

(cont'd)

Table 2 - cont'd.

- Longitudinal Edgewise Excitation (Ξ_{ϵ_x}):

c_{53}: $-K_a\Omega R(2\lambda T_{20} + \theta_{.75R} T_{21})\dot{\theta}_{x_f}$

k_{55}: $S_{49}(\omega_v^2 - \Omega^2)\epsilon_x$

k_{56}: $\left[2S_{49}\Omega\zeta_v\omega_v + K_a\Omega^2 R\left(2\frac{c_{d_o}}{a} T_{25} - \theta_{.75R}\lambda T_{24}\right)\right]\epsilon_y$

c_{57}: $[2\beta_B\Omega S_{25} - K_a\Omega R(2\lambda T_{22} + \theta_{.75R} T_{23})]\dot{\theta}_{x_R}$

- Lateral Edgewise Excitation (Ξ_{ϵ_y}):

c_{65}: $-2S_{49}\Omega\dot{\epsilon}_x$

k_{65}: $-\left[2S_{49}\Omega\zeta_v\omega_v + K_a\Omega^2 R\left(2\frac{c_{d_o}}{a} T_{25} - \theta_{.75R}\lambda T_{24}\right)\right]\epsilon_x$

k_{66}: $S_{49}(\omega_v^2 - \Omega^2)\epsilon_y$

- Rotor Rollwise Flatwise Excitation ($\Xi_{\theta_{x_R}}$):

m_{73}: $S_{12}\ddot{\theta}_{x_f}$

c_{73}: $K_a\Omega R T_{11}\dot{\theta}_{x_f}$

c_{75}: $[-2\beta_B\Omega S_{25} + K_a\Omega R(\lambda T_{22} + 2\theta_{.75R} T_{23})]\epsilon_x$

3.3 Flap-Lag Instability

The equations of motion selected for the analysis of flap-lag instability are those of Peters (Ref. 2, with updates transmitted to the author informally). These equations are essentially those published earlier by Ormiston and Hodges for hovering flight (Ref. 1) but with extensions which include (quasi-static) forward-flight aerodynamics. The inclusion of forward-flight aerodynamics produces periodicity in the equations of motion and, hence, admit the optional use of Floquet theory for solution.

Briefly, the (2 × 2) equations describe the coupled motion of the blade in rigid body flapping β, and lead-lag, ζ. These degrees-of-freedom, as elastically coupled by a general root retention spring system, constitute an idealization of the flapwise and inplane bending of a hingeless rotor blade with structural coupling arising from a variety of sources: pitch angle, twist, etc. The idealized elastic coupling is quantified using the uncoupled nonrotating natural frequencies in flap and lead-lag, ω_β and ω_ζ, respectively, and an elastic coupling factor, R. The Peters analysis also generalizes the automatic pitch change description to include both flapping and lead-lag effects, θ_β and θ_ζ, respectively. Finally, in addition to the aforementioned forward-flight aerodynamics effects, the analysis makes provision for investigating the effects of a partial trim. The trim calculation must be deemed only a partial trim in that it neglects the rotor inplane forces and assumes a zero shaft angle. Hence, in the numerical results presented propulsive force trim was omitted and only those control angles required for thrust and zero hub moment were calculated. The actual equations used for obtaining the partial trim conditions are given in Refs. 10 and 11.

These flap-lag equations are considerably simpler than those for air resonance in that there is no difficulty in identifying the critical

degrees-of-freedom and in establishing the energy-flow path. There are only four (4) off-diagonal terms which can couple these two degrees-of-freedom, and for zero elastic coupling (R = 0), the two off-diagonal damping matrix elements dominate. In order to clarify the discussion to follow, the damping matrix of the flap-lag equations is reproduced herein from Ref. 2 for the case of constant coefficients and zero flapping:

$$[C] = \begin{bmatrix} \frac{\gamma}{8} & \frac{2\beta_o}{+\frac{\gamma}{8}\left(\bar{\varphi} - 2\theta_o - \frac{4}{3}\mu\theta_s\right)} \\ \frac{-2\beta_o}{+\frac{\gamma}{8}\left(-2\bar{\varphi} + \theta_o + \frac{2}{3}\mu\theta_s\right)} & \frac{\gamma}{8}\left(2\frac{c_{d_o}}{a} + \theta_o\bar{\varphi} + \frac{2}{3}\mu\beta_o\theta_c\right) \end{bmatrix} \tag{22}$$

The increased complexity of the flap-lag instability problem over that of air resonance arises because of the periodicity of the coefficients. For this case it is possible for otherwise stabilizing or neutrally stable forces to act as drivers, as will be shown in the material to follow.

The FPM technique was applied to the flap-lag instability phenomenon using four basic flight conditions:

(1) Hovering ($\mu = 0$)
(2) Autorotation ($\mu = 0$)
(3) Forward-flight at $\mu = 0.3$
(4) Forward-flight at $\mu = 0.45$.

Additionally, the two forward-flight cases were run without and with the harmonic terms (i.e., constant coefficients vs. periodic coefficients). For all the cases, except where varied and so noted, the calculations were made using the following configuration parameters: $\omega_\beta = 0.3873$, $\omega_\zeta = 1.4$, $\gamma = 5$, $R = 0$, $C_T/\sigma = 0.2$, $\theta_\beta = \theta_\zeta = \theta_c = 0$, $c_{d_o} = 0.01$, $a = 2\pi$. The results of the calculations for these four cases are summarized in Table 3.

The bottom portion of Table 3 presents the stability results achieved both in terms of the critical eigenvalue (inplane motion dominant) and those elements of the force-phasing matrices which indicate that the corresponding terms in the equations of motion are drivers. All of the critical eigenvalue results calculated are consistent with those calculated and presented by Peters (Ref. 2). For those cases wherein Floquet theory was used (3b and 4b) the critical eigenvalues were calculated from the critical characteristic multipliers using the technique of Ref. 7. The variations in advance ratio μ, and inplane natural frequency ω_ζ, were selected so as to obtain results which showed instability, as well as demonstrated interesting facets of the FPM technique.

3.3.1 Non-Forward-Flight Cases ($\mu = 0$)

For the nominal inplane frequency of 1.4 the basic hovering case (1a) was found to be stable (again consistent with Refs. 1 and 2). Upon changing this frequency to 1.2 (case 1b), an instability was obtained and the drivers for the motion were found to be only those indicated by the (1,2) and (2,1) elements of the damping force-phasing matrix. Note that

TABLE 3

STABILITY AND FPM RESULTS FOR FLAP-LAG INSTABILITY CASES

Parameter	Case						
	1a	1b	2	3a	3b	4a	4b
μ	0	0	0	0.3	0.3	0.45	0.45
θ_o	17.02	17.02	10.41	14.90	14.90	17.53	17.53
θ_s	0	0	0	-10.90	-10.90	-20.02	-20.02
$\bar{\varphi}$	.0943	.0943	-.0083	.0222	.0222	.0148	.0148
β_o	5.49	5.49	5.14	5.20	5.20	5.14	5.14
ω_v	1.4	1.2	1.4	1.3	1.3	1.4	1.4
Harmonic terms	N	N	N	N	Y	N	Y
Result item							
λ_{crit}	-.00085 ±i1.398	.00072 ±i1.196	.00074 ±i1.399	.00020 ±i1.298	.00113 ±i1.299	-.00085 ±i1.398	.00219 ±i1.402
$p^o_{C_{12}}$	STABLE	1.00	1.00	1.00	1.05	STABLE	0.793
$p^o_{C_{21}}$		1.07	2.43	1.16	1.33		1.47
$p^o_{K_{11}}$		(-.00093)	(-.00070)	(-.00022)	0.23		1.24
$p^H_{C_{21}}$		-	-	-	.049		(-.031)
$p^H_{K_{21}}$		-	-	-	0.94		0.55

the (1,1) elements of the stiffness force-phasing matrix for these cases are negative and parenthesized to indicate that they are nondrivers or "quenchers."

In order to gain understanding of the basic instability mechanism, a parameter variation was made of the lead-lag frequency, ω_ζ, for the selected hovering flight condition. Figure 4 presents the results of this variation. The figure shows the variations of the stability indicating real part of the critical eigenvalue, the phasing of the flapping motion relative to the lead-lag motion, and the two driver elements of the damping force-phasing matrix with this lead-lag frequency. For variations in ω_ζ it can be seen from Eq.(22) that the off-diagonal damping matrix elements are invariant. Thus, the wide variation of $p^o_{C_{12}}$ and $p^o_{C_{21}}$ with ω_ζ must be due to the variation in the modal relationship of $\bar{\beta}$ to $\bar{\zeta}$, as shown by $\arg(\bar{\beta}/\bar{\zeta})$. Note that $p^o_{C_{12}}$ and $p^o_{C_{21}}$ correlate well with σ_{crit}, confirming the consistent role of the c_{12} and c_{21} terms as critical drivers. For this hovering condition the numerical evaluation of the [C] matrix is as follows:

$$[C] = \begin{bmatrix} 0.625 & -.121 \\ -.124 & .0195 \end{bmatrix}$$

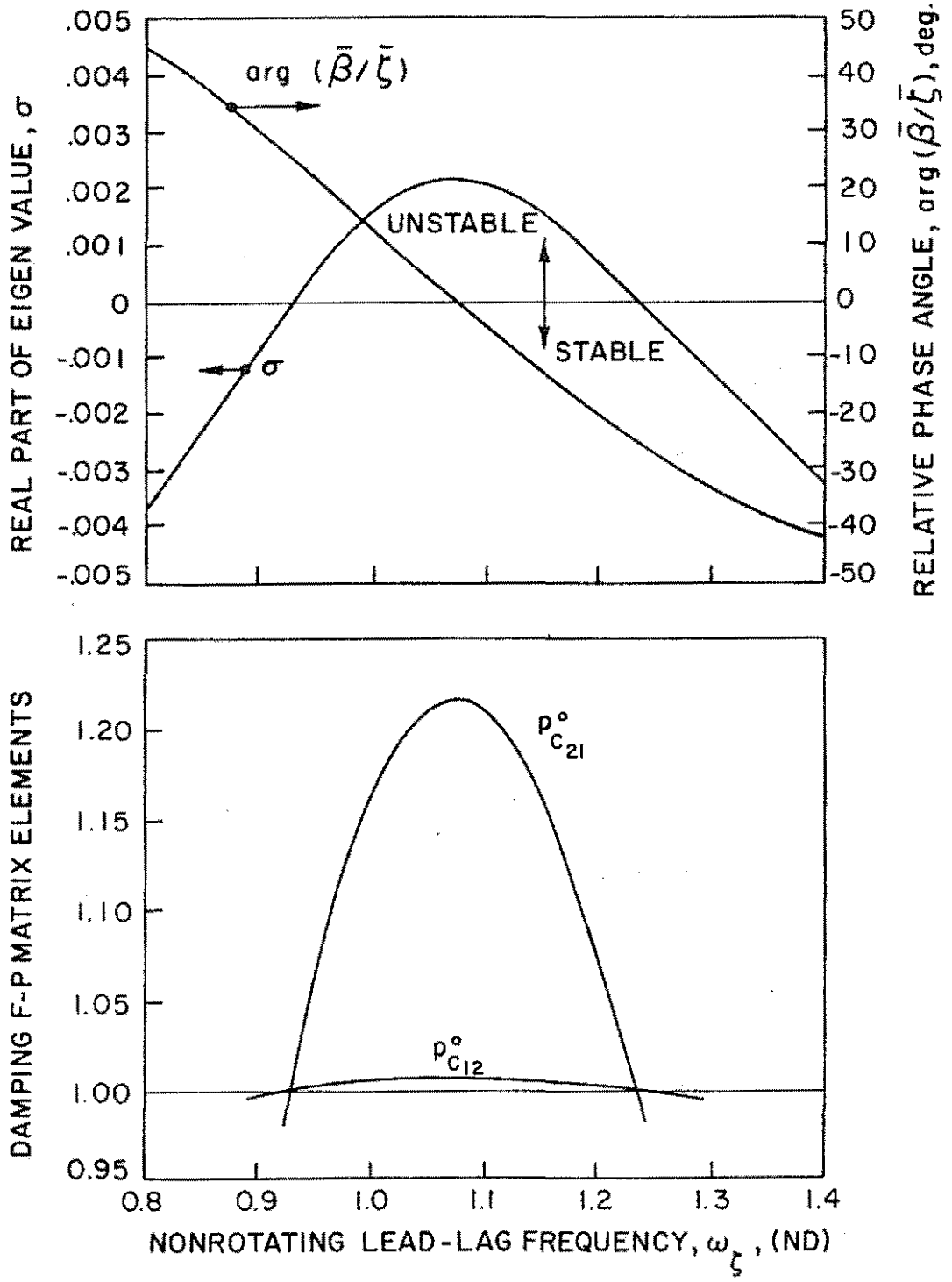

Figure 4 Variation of Flap-Lag Stability Parameters, Hovering Flight Condition, $C_T/\sigma = 0.2$, $\theta_o = 17.02$ deg, $\bar{\varphi} = 0.0943$

Figure 4 indicates that the maximum instability point occurs when the flapping and lead-lag motions are in-phase with each other. Thus, the role of these off-diagonal damping matrix elements becomes clearly that of being sources of negative damping. Note from Eq.(22) that the c_{12} damping matrix term would normally be positive ($= +2\beta_o$) but for the aerodynamic contribution, which becomes increasingly negative with θ_o. The trend of

decreasing stability with increasingly high values of collective angle is well recognized (Ref.1). The variation of the c_{21} term with θ_o, and correspondingly with $\bar{\varphi}$, however, is not nearly as great, and that element generally remains negative.

For the nominal lead-lag frequency the autorotational case (2) was found to be unstable verifying the destabilizing trend found for autorotative flight (Refs.10 and 11). Note that in the formulations of the FPM technique an arbitrary normalization of the matrices by the diagonal damping forces was employed. Thus the substantial increase in the $p^o_{C_{21}}$ damping force-phasing matrix element (= 2.43) over that for case 1a (=1.07) should be interpreted to mean either that the destabilizing impact of the c_{21} term in the equations has increased, and/or that the stabilizing impact of the c_{22} term has decreased. Examination of the damping matrix portion of the Peters equations, Eq.(22), indeed reveals a loss of inplane damping (c_{22}) with negative values of the inflow parameter $\bar{\varphi}$ at a rate higher than the accompanying reductions in the destabilizing damping matrix coupling terms (c_{12} and c_{21}). Thus, it would appear that the decrease in stability with autorotative flight, as reported in Refs.10 and 11, is principally due to the substantial loss of autogenous inplane damping arising from the change of sign on the inflow.

3.3.2 Forward Flight Cases ($\mu > 0$)

Each of the two selected forward-flight conditions was analyzed using both the constant coefficient approximate solution and the more exact Floquet/transition matrix solution. Note that for the periodic coefficient cases (3b and 4b) the FPM technique was applied separately to the constant portions of the system matrices as well as to the harmonic portions. The elements of the force-phasing matrices for these two components are denoted, respectively, by $(\ )^o$ and $(\ )^H$. Note also that for the higher advance ratio case the results again support the findings of Ref.2 that the inclusion of the periodic terms can reveal an instability which might be masked by the constant coefficient approximation. The lower advance ratio case (3b) required a reduction in ω_ζ to a value of 1.3 to achieve instability for both types of solution. Remarks made above concerning the hovering condition (case 1b) would appear to be applicable to the constant coefficient case (3a) as well and won't be repeated.

The results for the periodic coefficients case, however, show a somewhat different behavior. The off-diagonal coupling terms identified as critical drivers again include the (constant part of) the c_{12} and c_{21} damping terms, as before, but now with the harmonic portions of the c_{21} and k_{21} equation elements as well. A significant result is that the constant part of the diagonal k_{11} stiffening term is now acting as a driver, even though this term is always positive. Such a term could not act as a driver for the case of constant coefficients because of the constant phase and amplitude relationship between the characteristic velocity and displacement vectors (see Figure 1). However, for the case of periodic coefficients (Floquet theory) the phase and amplitude relationship between these two vectors is generally also periodic [12]. Thus, over one period it is possible for the characteristic displacement vector to

have (on the average) a component out-of-phase with velocity, and thus act as a negative damper. The details of this relationship as it applies to the flap-lag instability phenomenon are not yet well understood, however, and more study remains.

4. Concluding Remarks

Formulations have been presented which extend the range of applicability of the Force-Phasing Matrix (FPM) to include linear dynamic systems with both constant and periodic coefficients. The FPM technique should be viewed as a principal part of the eigensolution results. While it does not, by itself, indicate stability levels, such as are provided by the eigenvalues, it does provide insight into the physics of the instability. As such, it is much more directly useful than the basic eigenvector results, which are often disregarded because they are difficult to interpret. The implementation of the FPM technique as part of the eigensolution is quite simple. All of the results calculated for this study were computed using an IBM Personal Computer with a state-of-the-art FORTRAN compiler [13].

It should be stressed that the FPM technique is most properly used with and in support of engineering judgement; the results should be interpreted generally in the context of the specific application. The technique will usually not in of itself provide the design engineer with direct information as to how to stabilize any and all instabilities, much less in the most efficient manner. Its use lies more in providing the ability to identify those coupling terms which are drivers, to be reduced hopefully, and those which are quenchers, to be augmented, if possible.

From the numerical results of applying the FPM technique to the air resonance and flap-lag instability phenomena, the following specific conclusions have been drawn:

1. Ground resonance and air resonance instabilities are similar in that both require an energy-flow path between longitudinal and lateral cyclic rotor mode displacements of blade edgewise bending and both involve inertia couplings of the blade edgewise motion (accelerations) to the pylon motion force equilibrium.
2. Ground and air resonance are dissimilar in that the energy-flow paths for air resonance are multiple (both direct and indirect), rather than singular and do not involve inertia couplings of the pylon motion (accelerations) to the blade inplane motion force equilibrium, as with ground resonance.
3. Stabilization of the air resonance instability using the FPM technique would be difficult using only the basic passive coupling terms given in the simplified dynamic equations since they are not subject to significant independent variation. Successful stabilization using FPM might best be accomplished by investigating the impact of additional coupling parameters unrelated to aerodynamic performance which could be built into the system.
4. Simple flap-lag instability is basically caused by the off-diagonal damping elements. Of particular importance are those portions thereof relating to flapping airloads resulting from lead-lag velocity and inplane Coriolis (inertia) loads resulting from flapping velocity.

5. Flap-lag instability is characterized by flapping being closely in-phase with lead-lag. With this phase relationship and at relatively high blade pitch angles, the resulting loss of blade aerodynamic flap damping is a principal cause of flap-lag instability.

6. The reduction in flap-lag stability for autorotational flight is principally caused by the loss of autogenous inplane aerodynamic damping. This loss arises from the change in sign of the inflow inherently characteristic of autorotational flight.

7. The general reduction in flap-lag stability in forward flight, as predicted by Floquet theory vis-a-vis the constant coefficient approximation, is caused in part by the inconstant (periodic) phase relationship existing between flapping displacement and velocity for periodic coefficient systems. Such inconstancy of phase allows the otherwise neutrally stable, autogenous flapping stiffness (as defined by the constant coefficient part) to act as a significant driver in the blade flapwise motion moment equilibrium.

8. Further reductions in flap-lag stability in forward flight, again as predicted by Floquet theory, are caused by the harmonic (aerodynamic) stiffness coupling of flapping displacement in the lead-lag motion moment equilibrium.

References

1. R.A. Ormiston and D.H. Hodges, "Linear Flap-Lag Dynamics of Hingeless Helicopter Rotor Blades in Hover," Journal of the American Helicopter Society, 17, 2 (April 1972).

2. D.A. Peters, "Flap-Lag Stability of Helicopter Rotor Blades in Forward Flight," Journal of the American Helicopter Society, 20, 4 (October 1975).

3. R.T. Lytwyn, "Aeroelastic Stability Analysis of Hingeless Rotor Helicopters in Forward Flight Using Blade and Airframe Normal Modes," Proceedings of the 36th Annual National Forum of the American Helicopter Society, Paper No. 80-25, 1980.

4. R.L. Bielawa, "Techniques for Stability Analysis and Design Optimization with Dynamic Constraints of Nonconservative Linear Systems," Proceedings of the 12th AIAA/ASME Structures, Structural Dynamics and Materials Conference, Paper No. 71-388, 1971.

5. R.L. Bielawa, "Dynamic Analysis of Multi-Degree-of-Freedom Systems Using Phasing Matrices," Proceedings of Specialists' Meeting on Rotorcraft Dynamics, Ames Research Center, 1974.

6. J.A. Eisele and R.M. Mason, Applied Matrix and Tensor Analysis, Wiley-Interscience, New York, 1970.

7. P. Friedmann, C.E. Hammond and T-H. Woo, "Efficient Numerical Treatment of Periodic Systems with Application to Stability Problems," International Journal for Numerical Methods in Engineering, 11, 7 (1977).

8. R.L. Bielawa, "An Improved Technique for Testing Helicopter Rotor-Pylon Aeromechanical Stability Using Rotor Dynamic Impedance Characteristics," Vertica, 9, 2 (1985).

9. R.P. Coleman and A.M. Feingold, Theory of Self-Excited Mechanical Oscillations of Helicopter Rotors with Hinged Blades, NACA TR 1351, 1958.

10. F.-S. Wei, "Flap-Lag Stability of Helicopter and Windmill Rotor Blades in Powered Flight and Autorotation by a Perturbation Method," Doctor of Science Thesis, Washington University, St. Louis, 1978.

11. F.-S. Wei and D.A. Peters, "Lag Damping in Autorotation by a Perturbation Method," Proceedings of the 34th Annual National Forum of the American Helicopter Society, Paper No. 78-25, 1978.

12. T.L. Saaty and J. Bram, Nonlinear Mathematics, McGraw-Hill, New York, 1964.

13. Fortran IV Extended-User's Manual, IBM PC DOS Compatible (Version 2.10), Super Soft/Small Systems Services, Inc., Urbana, Illinois, 1985.

Nomenclature

a	Airfoil section lift curve slope, 1/deg
b	Number of blades
C_T/σ	Rotor thrust coefficient per blade solidity
c	Blade chord, cm
c_{d_o}	Airfoil section minimum drag coefficient
c_f	Pylon effective translational damping at hub, N-s/m
EI	Blade bending stiffness, N-m^2
F_{x_f}, F_{y_f}	Hub force excitations in x- and y-directions, respectively, N
f_n	Resultant driving force for nth degree-of-freedom, Eq.(3)
$[H(T-mh)]$	Matrix relating solution for two consecutive augmented state vectors (Ref.7)
Ⓗ	Hadamard or element by element matrix multiplication (Ref.6)
h_1	Distance airframe c.g. is below rotor hub, m
$I_{\theta_f}, I_{\varphi_f}$	Airframe pitch and roll inertias, respectively, about airframe c.g., kgm^2
K_A	Aerodynamic effectivity, kg-m
k_f	Pylon effective translational stiffness at hub, N/m
$[M],[C],[K]$	Inertia, damping and stiffness matrices, respectively
M_{x_f}, M_{y_f}	Hub moment excitations in roll and pitch, respectively, N-m
m_f	Airframe (pylon) mass, kg
m_{ij}, c_{ij}, k_{ij}	Elements of the [M], [C] and [K] matrices, respectively
m_R	Rotor mass, Kg
m'	Blade mass distribution, kg/m
N_p	Number of intervals into which period is divided
$[P_M^{(k)}], [P_C^{(k)}], [P_K^{(k)}]$	Force-Phasing Matrices for kth eigenvalue
R	Rotor radius, m, or elastic coupling parameter (Ref.2), as appropriate
r	Blade spanwise variable, m
$S_1, \ldots S_{49}$	Blade mass modal integration constants, as appropriate
T	Period defining periodicity of equation coefficients, or thrust, as appropriate
$T_1, \ldots T_{25}$	Blade aerodynamic modal integration constants, as appropriate
t	Time, sec
$[U^{(A)}], [U^{(B)}], [U^{(C)}]$	Matrices used to define characteristic acceleration, velocity and displacement vectors, respectively
x, y	Longitudinal and lateral hub displacements, respectively, m
$\{x\}$	Vector of system degrees-of-freedom
$\{y\}$	Augmented state vector
$\{y(0)\}$	Eigenvector of transition matrix
z	Complex hub displacement (= x + iy)
β_s	Blade precone angle, deg
β_0	Constant component of equilibrium flapping angle, deg.
γ	Blade Lock number
γ_v, γ_w	Blade 1st edgewise and flatwise bending mode shapes, respectively
e_x, e_y	Cyclic rotor mode descriptions of blade edgewise bending in Longitudinal and lateral directions, respectively
ζ_v, ζ_w	Blade structural damping equivalent critical damping ratios for edgewise and flatwise bending, respectively
θ_c, θ_s	Cosine and sine components of cyclic pitch control, deg
θ_k	Angular argument of kth (complex) eigenvalue, deg

$\theta_{x_f}, \theta_{y_f}$	Hub roll and pitch motion, respectively, deg
$\theta_{x_R}, \theta_{y_R}$	Cyclic rotor mode descriptions of blade flatwise bending in roll and pitch directions, respectively
$\theta_0, \theta_{.75R}$	Alternate forms of blade collective angle, deg
Λ_k	kth characteristic multiplier
λ	Alternatively, rotor inflow and Laplace transform space eigenvalue ($= \sigma \pm i\omega$), 1/sec
μ	Rotor advance ratio
ρ	Air density, kg/m^3
σ	Real part of system eigenvalue, giving stability information, 1/sec
$[\Phi(\psi,0)]$	Fundamental or generalized transition matrix for initial conditions given at $\psi = 0$
$[\Phi(T,0)]$	Transition matrix relating conditions at end of period to initial conditions
$[\varphi^{(k)}]$	kth eigenvector of dynamic matrix equation
$\bar{\varphi}$	Inflow parameter, $= \frac{4}{3}\lambda$
ψ	Alternatively, rotor azimuth angle and nondimensional time ($= \Omega t$)
Ω	Rotor speed, rad/sec
ω	Imaginary part of eigenvalue giving coupled frequency information, rad/sec
ω_v, ω_w	Inplane and flapwise (first) natural frequencies, respectively, of rotating elastic blade at $\theta_0 = 0$, 1/sec
$\omega_\beta, \omega_\zeta$	Dimensionless nonrotating flap and lead-lag frequencies of blade at $\theta_0 = 0$

Superscripts

$(\ )^{(a)}$	Arising from aerodynamic sources
$(\ )^H$	Pertaining to harmonic portion of periodic coefficients
$(\ )^{(k)}$	Relating to kth eigenvalue
$(\ )^0$	Pertaining to constant portion of periodic coefficients
$\bar{(\ )}$	Nondimensionalization by radius, R
$\overset{*}{(\ )}$	Differentiation with respect to ψ

Subscripts

$(\ )_{crit}$	Critical or unstable eigenvalue
$(\ )_m$	Conditions at mth instant of time within a period
$(\ )_v, (\ )_w$	Relating to blade edgewise and flatwise bending, respectively
$(\ )_x, (\ )_y$	In longitudinal and lateral directions, respectively

Appendix A - Characteristic Responses for Linear Systems with Periodic Coefficients

The eigenvalue problem resulting from the transition matrix approach to the stability solution of linear equations with periodic coefficients yields a set of k characteristic multipliers Λ_k, and a set of k characteristic vectors, $\{y(0)^k\}$. These vectors can be considered to be the k characteristic initial condition vectors. The problem of defining the characteristic responses (acceleration, velocity and displacement) at arbitrary instances within the system period can be obtained using the fundamental or generalized transition matrix $[\Phi(\psi_m,0)]$. This matrix relates the solution vector at an arbitrary instant, ψ_m, to that at $\psi = 0$:

$$\{y(\psi_m)\} = [\Phi(\psi_m,0)]\{y(0)\} \tag{A.1}$$

This generalized transition matrix is directly available in the calculation for $[\Phi(T,0)]$ (see Ref.7). Equation (A.1) can be rewritten using a partitioned form of a more compact notation for the generalized transition matrix:

$$\{y(\psi_m)\} = \begin{Bmatrix} \overset{*}{x}(\psi_m) \\ \hline x(\psi_m) \end{Bmatrix} = [\Phi(\psi_m,0)]\{y(0)\} = \begin{bmatrix} D1_m \\ \hline D2_m \end{bmatrix} \{y(0)\} \tag{A.2}$$

This equation together with Eqs.(10) and (12) then enable the U_m matrices of Eqs.(14a-b) to be written as

$$[U_m^{(A)}] = -[M]^{-1}\left[[C(\psi_m)][D1_m] + [K(\psi_m)][D2_m]\right] \tag{A.3}$$

$$[U_m^{(B)}] = [D1_m] \tag{A.4}$$

$$[U_m^{(C)}] = [D2_m] \tag{A.5}$$

Appendix B - Simplified Dynamic Equations for Ground and Air Resonance

The simplified equations of motion presented in this appendix are intended as a reasonably representative analytical vehicle for application of the Force-Phasing Matrices technique. As such, they are not intended for general analysis applications in support of actual helicopter design efforts. They are presented herein without mathematical development or justification.

The eight differential equations respectively model the responses in hub x- and y-translations, hub roll and pitch rotations, blade cyclic edgewise bending rotor modes in the x- and y-directions, and blade cyclic flatwise bending rotor modes in roll and pitch directions:

Hub Longitudinal Force (F_x)

$$(m_{f_x}+m_R)\ddot{x}+c_{f_x}\dot{x}+k_{f_x}x+(b\beta_B S_1 - m_f h_1)\ddot{\theta}_{y_f} + \frac{b}{2}\beta_B S_{16}\ddot{\theta}_{y_R} + \frac{b}{2}S_{48}\ddot{\epsilon}_x - T\theta_{y_f} = F_x^{(a)} \tag{B.1a}$$

Hub Lateral Force (F_y)

$$(m_{f_y}+m_R)\ddot{y}+c_{f_y}\dot{y}+k_{f_y}y - (b\beta_B S_1 - m_f h_1)\ddot{\theta}_{x_f} - \frac{b}{2}\beta_B S_{16}\ddot{\theta}_{x_R} + \frac{b}{2}S_{48}\ddot{\epsilon}_y + T\theta_{x_f} = F_y^{(a)} \tag{B.1b}$$

Hub Roll Moment (M_{x_y}

$$-(b\beta_B S_1 - m_f h_1)\ddot{y}+\left[I_{\varphi_f}+m_f h_1^2+\frac{b}{2}S_2(1+\beta_B^2)\right]\ddot{\theta}_{x_f}+\frac{b}{2}S_{12}\ddot{\theta}_{x_R} + 2\Omega\left(\frac{b}{2}\right)S_2\dot{\theta}_{y_f}+2\Omega\left(\frac{b}{2}\right)S_{12}\dot{\theta}_{y_R}-\beta_B\left(\frac{b}{2}\right)S_{46}\ddot{\epsilon}_y+m_f g h_1\theta_{x_f}=M_{x_f}^{(a)} \tag{B.1c}$$

Hub Pitch Moment (M_{y_f})

$$(b\beta_B S_1 - m_f h_1)\ddot{x} + \left[I_{\theta_f} + m_f h_1^2 + \frac{b}{2} S_2(1+\beta_B^2)\right]\ddot{\theta}_{y_f} + \frac{b}{2} S_{12}\ddot{\theta}_{y_R}$$

$$- 2\Omega\left(\frac{b}{2}\right)S_2\dot{\theta}_{x_f} - 2\Omega\left(\frac{b}{2}\right)S_{12}\dot{\theta}_{x_R} + \beta_B\left(\frac{b}{2}\right)S_{46}\ddot{\epsilon}_x + m_f g h_1 \theta_{y_f} = M^{(a)}_{x_y} \qquad \text{(B.1d)}$$

Rotor Longitudinal Edgewise Excitation (Ξ_{ϵ_x})

$$S_{48}\ddot{x} + \beta_B S_{46}\ddot{\theta}_{y_f} + S_{49}[\ddot{\epsilon}_x + 2\zeta_v\omega_v\dot{\epsilon}_x + (\omega_v^2 - \Omega^2)\epsilon_x]$$

$$+ S_{49}\Omega(2\dot{\epsilon}_y + 2\zeta_v\omega_v\epsilon_y + 2\beta_B\Omega S_{25}(\dot{\theta}_{x_R} + \Omega\theta_{y_R}) = \Xi^{(a)}_{\epsilon_x} \qquad \text{(B.1e)}$$

Rotor Lateral Edgewise Excitation (Ξ_{ϵ_y})

$$S_{48}\ddot{y} - \beta_B S_{46}\ddot{\theta}_{x_f} + S_{49}[\ddot{\epsilon}_y + 2\zeta_v\omega_v\dot{\epsilon}_y + (\omega_v^2 - \Omega^2)\epsilon_y]$$

$$- S_{49}\Omega(2\dot{\epsilon}_x + 2\zeta_v\omega_v\epsilon_x) + 2\beta_B\Omega S_{25}(\dot{\theta}_{y_R} - \Omega\theta_{x_R}) = \Xi^{(a)}_{\epsilon_y} \qquad \text{(B.1f)}$$

Rotor Rollwise Flatwise Excitation ($\Xi_{\theta_{x_R}}$)

$$-\beta_B S_{16}\ddot{y} + S_{12}(\ddot{\theta}_{x_f} + 2\Omega\dot{\theta}_{y_f}) + S_{10}[\ddot{\theta}_{x_R} + 2\zeta_w\omega_w\dot{\theta}_{x_R} + (\omega_w^2 - \Omega^2)\theta_{x_R}]$$

$$+ S_{10}\Omega(2\dot{\theta}_{y_R} + 2\zeta_w\omega_w\theta_{y_R}) - 2\beta_B\Omega S_{25}(\dot{\epsilon}_x + \Omega\epsilon_y) = \Xi^{(a)}_{\theta_{x_R}} \qquad \text{(B.1g)}$$

Rotor Pitchwise Flatwise Excitation ($\Xi_{\theta_{y_R}}$)

$$\beta_B S_{16}\ddot{x} + S_{12}(\ddot{\theta}_{y_f} - 2\Omega\dot{\theta}_{x_f}) + S_{10}[\ddot{\theta}_{y_R} + 2\zeta_w\omega_w\dot{\theta}_{y_R} + (\omega_w^2 - \Omega^2)\theta_{y_R}]$$

$$- S_{10}\Omega(2\dot{\theta}_{x_R} + 2\zeta_w\omega_w\theta_{x_R}) - 2\beta_B\Omega S_{25}(\dot{\epsilon}_y - \Omega\epsilon_x) = \Xi^{(a)}_{\theta_{y_R}} \qquad \text{(B.1h)}$$

where the various (inertia) integration constants are defined as follows:

$$S_1 = \int_0^R m'r\,dr \qquad S_{12} = R\int_0^R m'r\gamma_w\,dr \qquad S_{46} = R\int_0^R m'r\gamma_v\,dr$$

$$S_2 = \int_0^R m'r^2\,dr \qquad S_{16} = R\int_0^R m'\gamma_w\,dr \qquad S_{48} = R\int_0^R m'\gamma_v\,dr \qquad \text{(B.2a-i)}$$

$$S_{10} = R^2\int_0^R m'\gamma_w^2\,dr \qquad S_{25} = R^2\int_0^R m'\gamma_w\gamma_v\,dr \qquad S_{49} = R^2\int_0^R m'\gamma_v^2\,dr$$

Note that this equation set is intended for dual purpose in modeling both ground and air resonance characteristics. For ground resonance applications, only Eqs.(B.1a,b,e,f) are used, with the $\underline{(\,)}$ terms suppressed. For air resonance applications, all the equations are used, but with the $\underline{(\,)}$ terms suppressed.

The aerodynamic excitations, indicated by the $(\,)^{(a)}$ superscripted terms on the right-hand side of Eqs.(B.1a-h), were formed using simple quasi-static aerodynamic theory. To this end the static lift curve slope a, a uniform constant drag coefficient c_{d_o}, built-in precone angle, β_B, the collective angle $\theta_{.75R}$, and uniform inflow λ, were included in the formulations. The more realistic effects of twist, air mass dynamics, lift deficiency and nonuniform inflow were omitted consistent with the intended use of the equations.

The simplified modeling of these aerodynamic terms is more or less standard and the explicit expressions for these terms are given below without derivation:

$$
\begin{aligned}
F_x^{(a)} = \frac{b}{2} K_a \Omega \Bigg\{ & -\left[\left(\beta_B^2 + 2\frac{c_{d_o}}{a}\right) T_2 - \theta_{.75R}\lambda T_1\right]\frac{\dot{x}}{R} \\
& - 3\beta_B(\lambda T_1 + \theta_{.75R} T_2)\frac{\dot{y}}{R} + (2\lambda T_2 + \theta_{.75R} T_3)\dot{\theta}_{x_f} \\
& - \beta_B T_3 \dot{\theta}_{y_f} - \left(2\frac{c_{d_o}}{a} T_{20} - \theta_{.75R}\lambda T_{19}\right)(\dot{\epsilon}_x + \Omega\epsilon_y) \\
& - \beta_B(\lambda T_{19} + 2\theta_{.75R} T_{20})(\dot{\epsilon}_y - \Omega\epsilon_x) \\
& + (2\lambda T_5 + \theta_{.75R} T_6)(\dot{\theta}_{x_R} + \Omega\theta_{y_R}) \\
& - \beta_B T_6(\dot{\theta}_{y_R} - \Omega\theta_{x_R}) + \Omega(\lambda T_8 + \theta_{.75R} T_{18})\theta_{y_R} \Bigg\}
\end{aligned}
\tag{B.3a}
$$

$$
\begin{aligned}
F_y^{(a)} = \frac{b}{2} K_a \Omega \Bigg\{ & 3\beta_B(\lambda T_1 + \theta_{.75R} T_2)\frac{\dot{x}}{R} \\
& - \left[\left(\beta_B^2 + 2\frac{c_{d_o}}{a}\right) T_2 - \theta_{.75R}\lambda T_1\right]\frac{\dot{y}}{R} + \beta_B T_3 \dot{\theta}_{x_f} \\
& + (2\lambda T_2 + \theta_{.75R} T_3)\dot{\theta}_{y_f} + \beta_B(\lambda T_{19} + 2\theta_{.75R} T_{20})(\dot{\epsilon}_x + \Omega\epsilon_y) \\
& - \left(2\frac{c_{d_o}}{a} T_{20} - \theta_{.75R}\lambda T_{19}\right)(\dot{\epsilon}_y - \Omega\epsilon_x) + \beta_B T_6(\dot{\theta}_{x_R} + \Omega\theta_{y_R}) \\
& + (2\lambda T_5 + \theta_{.75R} T_6)(\dot{\theta}_{y_R} - \Omega\theta_{x_R}) - \Omega(\lambda T_8 + \theta_{.75R} T_{18})\theta_{x_R} \Bigg\}
\end{aligned}
\tag{B.3b}
$$

$$M_{x_f}^{(a)} = \frac{b}{2} K_a \Omega R\Big\{-(\lambda T_2 + 2\theta_{.75R} T_3)\frac{\dot{x}}{R} + \beta_B T_3 \frac{\dot{y}}{R}$$

$$- T_4 \dot{\theta}_{x_f} - (\lambda T_{20} + 2\theta_{.75R} T_{21})(\dot{\epsilon}_x + \Omega\epsilon_y) - T_{11}(\dot{\theta}_{x_R} + \Omega\theta_{y_R})\Big\} \quad (B.3c)$$

$$M_{y_f}^{(a)} = \frac{b}{2} K_a \Omega R\Big\{-\beta_B T_3 \frac{\dot{x}}{R} - (\lambda T_2 + 2\theta_{.75R} T_3)\frac{\dot{y}}{R}$$

$$- T_4 \dot{\theta}_{y_f} - (\lambda T_{20} + 2\theta_{.75R} T_{21})(\dot{\epsilon}_y - \Omega\epsilon_x) - T_{11}(\dot{\theta}_{y_R} - \Omega\theta_{x_R})\Big\} \quad (B.3d)$$

$$\Xi_{\epsilon_x}^{(a)} = K_a \Omega R\Big\{-\Big(2\frac{c_{d_o}}{a} T_{20} - \theta_{.75R}\lambda T_{19}\Big)\frac{\dot{x}}{R}$$

$$- \beta_B(2\lambda T_{19} + \theta_{.75R} T_{20})\frac{\dot{y}}{R} + (2\lambda T_{20} + \theta_{.75R} T_{21})\dot{\theta}_{x_f}$$

$$- \Big(2\frac{c_{d_o}}{a} T_{25} - \theta_{.75R}\lambda T_{24}\Big)(\dot{\epsilon}_x + \Omega\epsilon_y)$$

$$+ (2\lambda T_{22} + \theta_{.75R} T_{23})(\dot{\theta}_{x_R} + \Omega\theta_{y_R})\Big\} \quad (B.3e)$$

$$\Xi_{\epsilon_y}^{(a)} = K_a \Omega R\Big\{\beta_B(2\lambda T_{19} + \theta_{.75R} T_{20})\frac{\dot{x}}{R}$$

$$- \Big(2\frac{c_{d_o}}{a} T_{20} - \theta_{.75R}\lambda T_{19}\Big)\frac{\dot{y}}{R} + (2\lambda T_{20} + \theta_{.75R} T_{21})\dot{\theta}_{y_f}$$

$$- \Big(2\frac{c_{d_o}}{a} T_{25} - \theta_{.75R}\lambda T_{24}\Big)(\dot{\epsilon}_y - \Omega\epsilon_x)$$

$$+ (2\lambda T_{22} + \theta_{.75R} T_{23})(\dot{\theta}_{y_R} - \Omega\theta_{x_R})\Big\} \quad (B.3f)$$

$$\Xi_{\theta_{x_R}}^{(a)} = K_a \Omega R\Big\{-(\lambda T_5 + 2\theta_{.75R} T_6)\frac{\dot{x}}{R} + \beta_B T_6 \frac{\dot{y}}{R}$$

$$- T_{11}\dot{\theta}_{x_f} - (\lambda T_{22} + 2\theta_{.75R} T_{23})(\dot{\epsilon}_x + \Omega\epsilon_y) - T_{13}(\dot{\theta}_{x_R} + \Omega\theta_{y_R})\Big\} \quad (B.3g)$$

$$\Xi_{\theta_{y_R}}^{(a)} = K_a \Omega R\Big\{-\beta_B T_6 \frac{\dot{x}}{R} - (\lambda T_5 + 2\theta_{.75R} T_6)\frac{\dot{y}}{R}$$

$$- T_{11}\dot{\theta}_{y_f} - (\lambda T_{22} + 2\theta_{.75R} T_{23})(\dot{\epsilon}_y - \Omega\epsilon_x) - T_{13}(\dot{\theta}_{y_R} - \Omega_{x_R})\Big\} \quad (B.3h)$$

where:

$$K_a = \frac{1}{2}\rho a R^4$$

and where the various (aerodynamic) integration constants are given by:

$$T_1 = \int_0^1 \bar{c}\, d\bar{r} = \left(\frac{c}{R}\right)_{avg} \qquad T_{18} = \int_0^1 \bar{c}\,\bar{r}^2 \gamma_w' d\bar{r}$$

$$T_2 = \int_0^1 \bar{c}\,\bar{r}\, d\bar{r} \qquad T_{19} = \int_0^1 \bar{c}\gamma_v d\bar{r}$$

$$T_3 = \int_0^1 \bar{c}\,\bar{r}^2 d\bar{r} \qquad T_{20} = \int_0^1 \bar{c}\,\bar{r}\,\gamma_v d\bar{r}$$

$$T_4 = \int_0^1 \bar{c}\,\bar{r}^3 d\bar{r} \qquad T_{21} = \int_0^1 \bar{c}\,\bar{r}^2 \gamma_v d\bar{r} \qquad \text{(B.5a-q)}$$

$$T_5 = \int_0^1 \bar{c}\gamma_w d\bar{r} \qquad T_{22} = \int_0^1 \bar{c}\gamma_v\gamma_w d\bar{r}$$

$$T_6 = \int_0^1 \bar{c}\,\bar{r}\,\gamma_w d\bar{r} \qquad T_{23} = \int_0^1 \bar{c}\,\bar{r}\,\gamma_v\gamma_w d\bar{r}$$

$$T_8 = \int_0^1 \bar{c}\,\bar{r}\,\gamma_w' d\bar{r} \qquad T_{24} = \int_0^1 \bar{c}\gamma_v^2 d\bar{r}$$

$$T_{11} = \int_0^1 \bar{c}\,\bar{r}^2 \gamma_w d\bar{r} \qquad T_{25} = \int_0^1 \bar{c}\,\bar{r}\,\gamma_v^2 d\bar{r}$$

$$T_{13} = \int_0^1 \bar{c}\,\bar{r}\,\gamma_w^2 d\bar{r}$$

Note that for integration constants T_8 and T_{18} the derivative of the flatwise mode shape, γ_w', is understood to be with respect to $\bar{r}$.